A cortex-like canonical circuit in the avian forebrain

Martin Stacho[1,5*,†], Christina Herold[2,†], Noemi Rook[1], Hermann Wagner[3], Markus Axer[4], Katrin Amunts[2,4] and Onur Güntürkün[1]

1. Ruhr-University Bochum, Institute of Cognitive Neuroscience, Faculty of Psychology, Department Biopsychology, 44801 Bochum, Germany
2. C. & O. Vogt-Institute for Brain Research, Medical Faculty, Heinrich Heine University of Düsseldorf, 40225 Düsseldorf, Germany
3. RWTH Aachen University, Institute for Biology II, Worringerweg 3, 52074 Aachen, Germany
4. Institute of Neuroscience and Medicine INM-1, Research Center Jülich, 52425 Jülich, Germany
5. Ruhr-University Bochum, Institute of Physiology, Faculty of Medicine, Department of Neurophysiology, Universitätsstraße 150, 44801 Bochum

† These authors contributed equally to the work and share first authorship.

Words in abstracts: 107

Words in article (incl. text body, references, captions, but excluding supplementary materials: 4.445

References: 40, plus 5 from citations in materials and methods

Figures: 6 plus 2 in supplementary materials

Classification: Biological Sciences - Neuroscience

*__Corresponding author:__
Martin Stacho
E-mail: Martin.Stacho@rub.de
Phone: +49 234 32 22042
Ruhr-University Bochum, Institute of Physiology, Faculty of Medicine, Department of Neurophysiology, Universitätsstraße 150, 44801 Bochum

Abstract

Birds achieve extraordinary cognitive skills that are comparable to mammals, although their pallium seems to lack an organization akin to cerebral cortex. Here, we analyzed the fiber architecture of the avian pallium with 3D-Polarized Light Imaging, and subsequently reconstructed local and associative pallial circuits with tracing techniques. We discovered an iteratively repeated, column-like neuronal circuitry across the layer-like nuclear boundaries of hyperpallium and dorsal ventricular ridge. These circuits are connected to neighboring columns and, via horizontal layer-like connections, to higher associative and motor areas. Our findings indicate that this avian canonical circuitry constitutes the structural basis of neuronal computation, and is stunningly similar to its mammalian counterpart.

Keywords: birds, dorsal ventricular ridge, pallium, hyperpallium, wulst, columns, layers, pigeon, owl, 3D-PLI

One Sentence Summary:

Birds versus mammals: Two differently shaped forebrain organizations use similar routes of neuronal micro-circuitry.

Mammals and birds share a common ancestor that lived about 320 million years ago. Since then, this ancestor's dorsal pallium developed in the mammalian lineage into the cerebral cortex. The cortex is composed of cortical layers which are horizontally organized as well as columns which run orthogonal to layers and thus create a vertical organization. Cortical layers contain different types of neurons, each with specific afferent and efferent connections. Layers and columns show a characteristic pattern in each cortical area, which is closely related to its connectivity and function. In birds, the last common ancestor's dorsal pallium developed into a nuclear structure called hyperpallium. This area is considered to be entirely (*1, 2*) or mostly (*3*) homologues to cortex. Most of the other avian pallial nuclei bulge below the lateral ventricle and are collectively called dorsal ventricular ridge (DVR).

The possible homologies of DVR to different parts of the mammalian pallium are controversial. Developmental and genetic studies come to diverse conclusions that reach from a field homology of the DVR to mammalian ventral and lateral pallium (*3, 4*) up to lamina- or cell-type based homologies to cortex (*1, 2, 5, 6*). The picture is different when long-range connections of hyperpallium and DVR are analyzed. These evince an astonishing similarity to ascending and descending cortical pathways (*1, 7*). Recently, also the local connectivity patterns of auditory and visual DVR-areas were shown to display layer- and column-like connectivity (*8–10*). These last findings open up the tantalizing possibility that at least some DVR components could display a cortex-like architecture.

We tested this hypothesis by posing three questions: (1) Does a microscale fiber architecture analysis of the entire avian sensory DVR and hyperpallium reveal a cortex-like pattern in two phylogenetically distant bird species like pigeon and barn owl? (2) Are the local connectivity patterns of these layer- and column-like architectures similar in both, DVR and hyperpallium? (3) Are there specific layers and cell populations in this matrix that give rise to long-range intrahemispheric connections akin to cortex?

The overall fiber architecture of the avian sensory pallium

To answer the first of these questions, we analyzed the overall fiber architecture in pigeons, starting with the DVR using 3D-Polarized Light Imaging, an optical technique that visualizes axons in unstained histological sections (3D-PLI) (Figs. 1, S1) (*11, 12*). The DVR harbors three primary sensory territories which, from anterior to posterior, are the trigeminal n. basorostralis pallii (BAS), the visual entopallium (E) and the auditory Field L (Fig. 1A, B). In the following, we use "horizontal" and "vertical" always with reference to the plane of the borderline between two pallial territories.

3D-PLI revealed a combination of mostly lamina-like and vertical fiber architectures of sensory DVR systems (Fig.1 C-I). Fig. 1D shows fibers of BAS and overlying nido- and mesopallium in different colors according to their spatial orientation. Parallel fibers were oriented perpendicularly to the dorsal

surface of BAS and crossed the frontal nidopallium towards the frontal mesopallium ventrale (MFV). The orthogonal organization of fibers in nidopallium frontotrigeminale (NFT) became particularly evident when only two orthogonal fiber orientations were visible (Fig. 1E). The same applied to the visual DVR system (Fig. 1C), where also vertical fibers between entopallium, nidopallium and mesopallium were organized in parallel columnar axon bundles with crossing horizontal fibers in nidopallium intermediale (NI) (Fig. 1C, F). 3D-PLI spotlight images, which are orientation maps that highlight specific fiber orientations, revealed only small fiber contingents if rotated by further 45° (Fig. 1G). A similar architecture was observed in auditory DVR where L1 fiber pattern was orthogonal to mesopallium caudomediale (CMM) (Fig 1H, I).

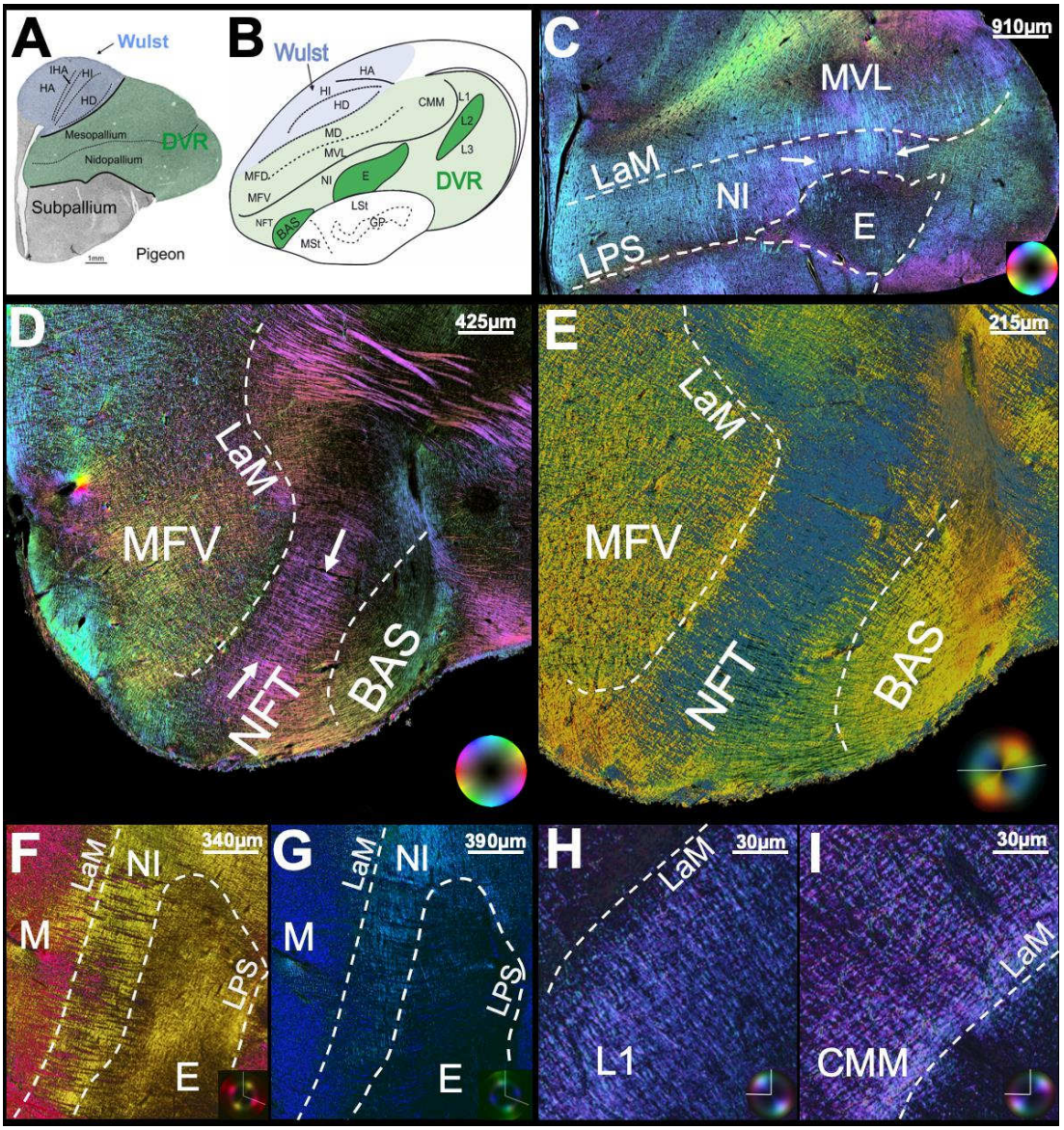

Figure 1) **3D fiber architecture of DVR**. A) Schematic localization of hyperpallium (blue) and DVR (green) in frontal and (B) sagittal plane of the pigeon's telencephalon. C) 3D-PLI frontal pallial image at

A11.25 (*13*) with color wheel hues indicating in-plane fiber orientations. Black denotes perpendicular inclination to plane. Arrows: fibers crossing through NI between E and MVL. D) 3D-PLI sagittal visualization of Bas-NFT-MFV (L3.70) with fibers crossing through NFT (arrows). E) Overlay of two 3D-PLI spotlight images (blue: 50°/230°±60° (direction ± inclination), orange: 140°/320°±60°) reveals fiber orthogonality. F) 3D-PLI sagittal entopallial region (L3.5) with orthogonal yellow and dark-pink fibers. G) Contrasting this pattern with two 3D-PLI spotlight images rotated by 45° (pink fibers: 30°/210°±60°, yellow: 120°/300°±60°). H) Perpendicular fiber orientations in L1 and (I) CMM become visible through 3D-PLI spotlight images rotated by 90° in a frontal section around A6.50 (H:40°/220°±50°; I: 130°/310°±50°).

We then turned our attention to the hyperpallium, where main fiber orientations differed between areas (Fig. 2A). While hyperpallium apicale (HA) and hyperpallium intercalatum (HI) showed several orientations of fibers, those in the interstitial nucleus of HA (IHA) and hyperpallium dorsale (HD) were mostly longitudinally oriented (Fig. 2A, B). Zooming into these areas by selectively highlighting orthogonal directions revealed fibers that were mostly, but not entirely, either parallel or orthogonal to hyperpallial areal borders (Fig. 2B-D).

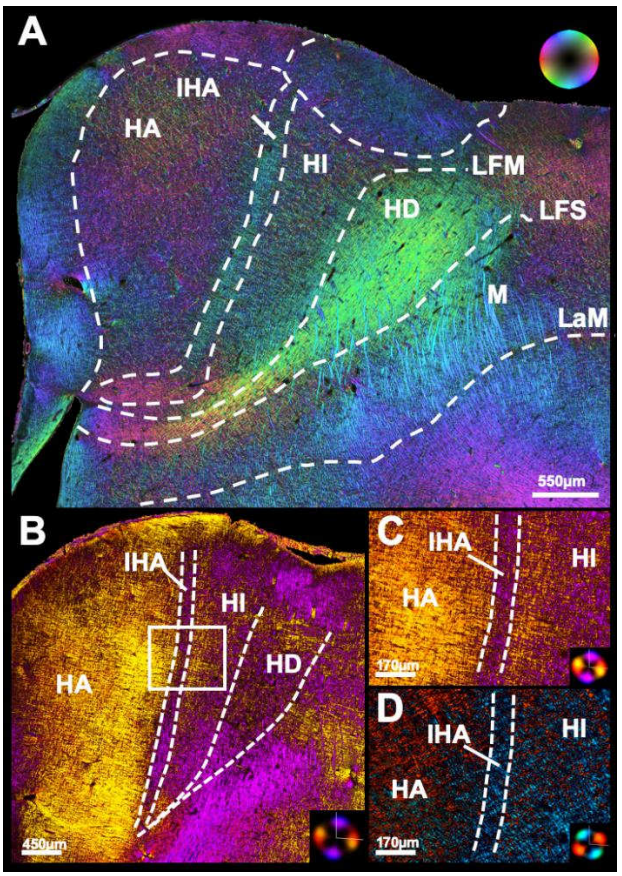

Figure 2) **Fiber architecture of pigeon hyperpallium.** A) Hyperpallial fiber orientations at A11.75. B) Overlay of two 3D-PLI spotlight images at A 12.50 showing two main orthogonal fiber orientations (purple: 100°/280°±50°, yellow: 10°/190°±50 degrees. C) Zoom into the white square. D) Smaller fiber

contingents remain when 3D-PLI spotlight images are rotated by 45° relative to Fig. 2B.

Local and long-range circuits in the avian sensory telencephalon

The 3D-PLI analyses revealed that fiber arrangements of sensory DVR and hyperpallium were mainly, although not exclusively orthogonal and thus resembled a cortex-like architype. However, another hallmark of the mammalian cortex is its repetitive canonical columnar circuitry. To answer question 2 and to reveal a possibly similar pattern, we used injections of in-vivo CTB (retrograde) and in-vitro biocytin tracing (retro- and anterograde) to reveal local connectivity patterns. Again, we started with the DVR.

In-vitro biocytin injections into the thalamopallial termination areas of the trigeminal (BAS), visual-tectofugal (E), and auditory streams (Field L2) revealed reciprocal projections to the ventral mesopallium (trigeminal: mesopallium frontoventrale, MFV; visual: mesopallium ventrolaterale, MVL; auditory: CMM) (Fig. 3A-C; S2A, C-E). These axons were constituted by parallel varicose fiber bundles of 15-70 µm diameter that gave rise to collateral branches (Fig. 3B; Fig. S2E). However, a minority of the ascending fibers continued further dorsally to also reach the dorsal extent of the mesopallium (trigeminal: mesopallium frontodorsale, MFD, visual: mesopallium dorsale, MD; auditory: dorsal CMM) (Fig. 3D, E; Fig. S2F). In the trigeminal and visual systems, Bas and E could be subdivided into ventral and dorsal subdivisions. The same applied for MFV and MVL with their ventral interna (MFVint, MVLint) and their dorsal externa division (MFVext, MVLext). With a series of minute injections, we revealed that entire Bas and E were connected to MFVext and MVLext, respectively (Fig. S2F). In addition, Bas and E as well as L2 innervated the lateral striatum (LSt) (Fig. S2F).

Furthermore, these injections also revealed projections to the adjacent nidopallial areas NFT, nidopallium intermediale NI, and fields L1/L3, respectively (Fig. 3A-C; S2A, D) (*7–10, 14*). These areas projected vertically back towards the primary sensory areas (Fig. 3G, H; S2B, F). However, trigeminal NFT, visual NI, and auditory L1 also evinced vertically ascending projections towards MFVext, MVLext, and CMM, respectively (Fig. S2F). Finally, these mesopallial areas also projected topographically back towards their trigeminal (NFT, Bas), visual (NI, E), and auditory targets (L1/L2) (Fig. 3E, F, I; S2C, E, F).

In addition to these column-like projections, many varicose fibers within NFT and NI run horizontally, thus creating a perfect grid-like pattern with vertically oriented columns (Fig. 3O, P; N; S2F). To reveal the connection of the horizontal system and to tackle question three concerning specific layers and cell populations that give rise to long-range connections, we combined in-vitro tracing with in-vivo injections of CTB into either associative NCL or pre/motoric arcopallium. The tracing experiments labelled numerous neurons in NI, NFT and L1. (Fig. 3J-N) (*7–10, 14*). As revealed by confocal

microscopy, NFT-, NI-, and L1-cells were presumably contacted by fibers ascending from the primary sensory areas of the respective DVR-systems (Fig. 3J-M). Thus, the sensory DVR-circuitry connects to NCL and arcopallium via horizontally projecting nidopallial neurons.

In summary, local DVR circuits were constituted by several horizontally stacked, layer-like areas across nido- and mesopallium and an orthogonal and column-like arrangement of iteratively organized reciprocal circuits with lamina-specific cell types (Fig. 3D, I, N). In addition, NI was characterized by horizontal projections to nearby columns as well as distant associative and motoric structures (*7*). Thus, such a connectivity confirms the orthogonal pattern revealed by 3D-PLI (Fig. 3Q, Fig. S2F).

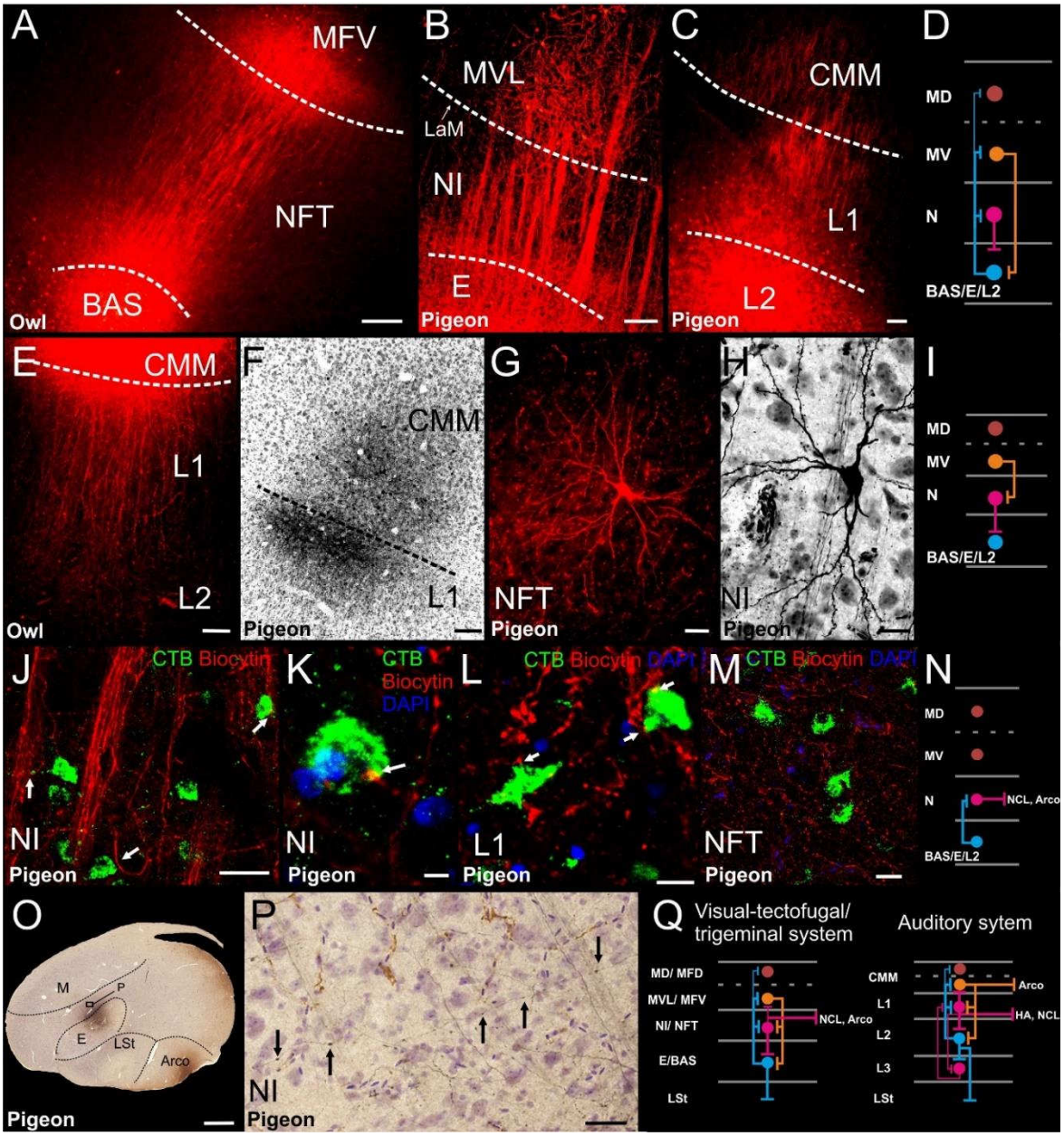

Figure 3) **Local circuitry of DVR**. Species is indicated on each figure. (A) BAS-injections label fibers running in parallel towards MFV. Retrogradely labelled neurons are visible in NFT and MFV. (B) Entopallium- and (C) L2-injections result in identical patterns in visual and auditory systems,

respectively. (D) Chart of connections shown in A-C. (E) Injections into CMM label fibers in columnar fashion as well as back-labelled neurons in L2 and L1. (F) Injection into L1 labels neurons and fibers in CMM. (G) NFT- and (H) NI-neurons (with Nissl counterstain) situated between parallel axons that project back to BAS and E, respectively. (I) Chart of connections shown in E-H. (J) Labelled fibers (red, biocytin) after E-injection surround NI-neurons (green, CTB) with lateral dendrites (arrows) after NCL-injection. (K) NCL-projecting NI-neuron (green) receives putative synaptic input (arrow) from bypassing E-fibers (red, biocytin). (L) NCL projecting L1-neurons contacted by bypassing L2→CMM fibers. (M) NFT-neurons (green) after CTB-injection into NCL are contacted by biocytin labelled BAS-fibers (red). (N) Chart of connections shown in J-M. (O) Nissl-stained section of an injection between E and NI. (P) Magnification of NI showing axons that run perpendicular to E→MVL-fibers. (Q) Schematic summary of the connections in the sensory DVR. Scale bars = 200µm (A), 10µm (B, H, L), 50µm (C, K), 500µm (E, F), 100µm (J), 20µm (G, M), 2mm (O), 25µm (P).

We investigated the hyperpallial connectivity along the whole anterior (somatosensory) to posterior (visual-thalamofugal) axis in owls and pigeons (Figs. 4, 5). The hyperpallium in owls is larger than in pigeons and we differentiated the thalamorecipient granular cell layer IHA in owls into inner (in-IHA) and outer (ex-IHA) bands, and the HA layer into dorsal and ventral HA (Fig. 5A).

We started with in-vitro biocytin injections into different positions of the pigeons' and owl's dorsal HA and revealed axons with multiple varicosities that were oriented perpendicular to hyperpallial layers and reached IHA, HI, and in pigeons also HD (Fig. 4A-D, Fig. 5D). These axons then continued into dorsal mesopallium and nidopallium frontolaterale (NFL). All hyperpallial layers also projected back onto HA with the strongest projection arising in pigeons from HD (Fig. 4R, 5B-F).

Biocytin in-vitro applications into the pigeons' IHA (Fig. 4F-I) resulted in vertical bands of beaded fibers within HA (Fig. 4G) and fewer in adjacent HI (Fig. 4H). When placing biocytin in-vitro into the thalamorecipient ex-IHA in owls, we revealed a columnar patch of retrogradely labelled neurons in in-IHA, HI, and ventral HA (Fig. 5B-F).

In-vitro biocytin injections into various positions of the pigeons' HI revealed perpendicularly ascending HI-projections to IHA and HA (Fig. 4K, L) and descending ones to HD. In owls, these experiments evinced labelled multiple HI-axons with varicosities within ex-IHA and ventral HA (Fig. 5E), topographically positioned retrogradely labelled HD- and broadly scattered HA-neurons (Fig. 5H). In-vivo CTB injections into the pigeon's HI resulted in retrogradely labelled neurons in HI, HA, HD, NFL, and MD (Fig. 4M).

In-vitro biocytin injections into various locations of HD in owls confirmed the perpendicular projection to HI and revealed further efferent fibers to the mesopallium. However, the strongest fiber labelling

was found within HD itself, where many fibers with large numbers of varicosities run horizontally along HD, thereby rarely crossing the HD boundary (Fig. 5G). The same experiment in pigeons also labelled perpendicularly ascending fibers containing varicosities and axon terminals within HI, IHA and HA (Fig. 4N-Q). In pigeons, a strong horizontal projection of HD-fibers was visible that was located at the HD/MD border (Fig. 4S, T).

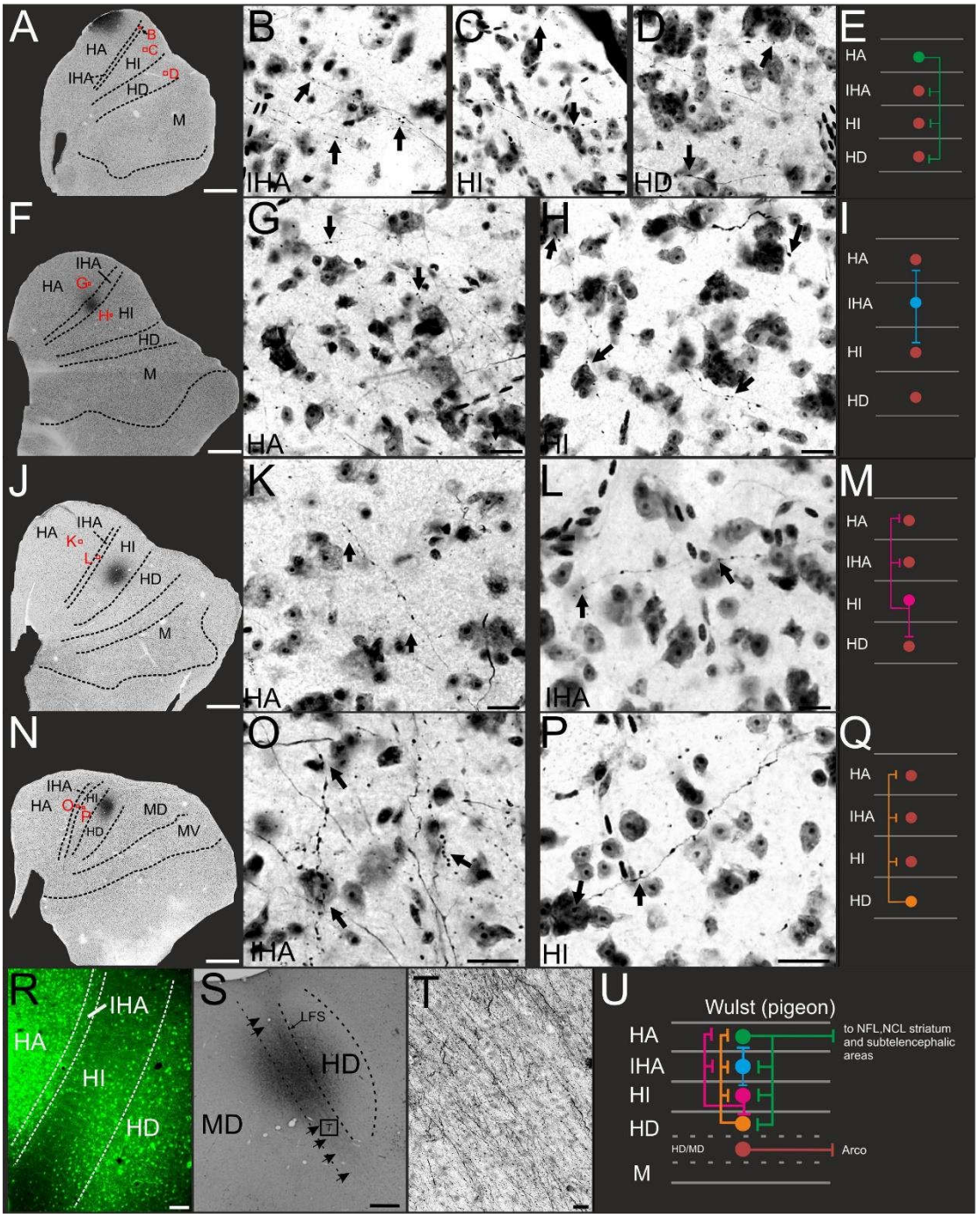

Figure 4) **Hyperpallial connectivity in pigeons**. A (HA), J (IHA), F (HI), and N (HD) depict Nissl stained sections with in-vitro biocytin injections into the respective region. The magnifications to the right of each case show varicosity-rich fibers and terminals found along a straight vertical extension to the

injection spot, perpendicular to the hyperpallial borderlines. Schemata on the right side (E, I, M, Q) depict the respective intra-hyperpallial projections. R) In-vivo CTB injection into HA with labelled fibers that are organized perpendicular to layers. Large numbers of neurons were retrogradely labelled within HD and less in HI. S) In-vitro injection at the HD/MD border with longitudinally running labelled fibers (magnification in T). U) Reconstructed intra-hyperpallial connectivity. Scale bar = 20µm (B-D, G, H, K, L, O, P, T); 100µm (R); 500µm (S), 1mm in A, F, J, N.

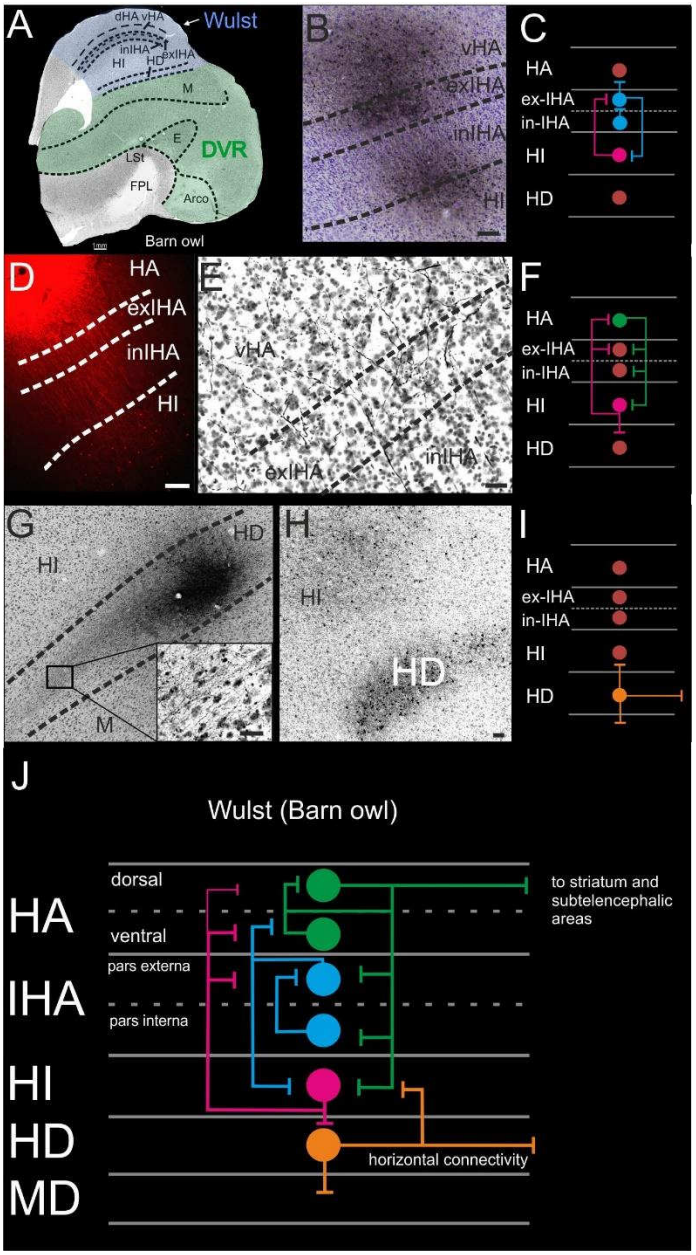

Figure 5) **Hyperpallial connectivity in barn owls**. A) Frontal section showing wulst (hyperpallium) and DVR. B) Injection into ex-IHA and vHA labelled neurons in in-IHA and dorsal HI. C) Schema of HI and IHA projections. D) In-vitro biocytin injection into HA labelled HI neurons with an orthogonal organization of fibers to layers. E) Terminations in ex-IHA and vHA observed after in-vitro biocytin

injections into HI. F) Schema of HI and HA projections. G) HD-injections evinced a strong longitudinal intralaminar HD-projection (insert shows higher magnification). H) HI-injections revealed that HD projected heavily to HI. I) Schema of HD projections. J) Summary of the wulst connections in the owl Scale bars: E=20µm; B, G (insert)=50µm; H=100µm; D=200µm.

The overall pattern of hyperpallial connectivity's are schematically shown in figures 4U and 5J and apply throughout the hyperpallial anteroposterior extent. Despite the different ecological specializations of barn owls and pigeons and the major phylogenetic distance between Strigiformes and Columbiformes (*15*), the two connectivity charts are astonishingly similar. Thus, these two species, and possibly other birds, possess similar hyperpallial repetitive canonical circuitries.

Discussion

The current study demonstrates that the architecture of the sensory avian pallium is dominated by two orthogonally oriented elements. The first consists of the parallel stacked lamina-like areas with their horizontal input zones and their horizontally organized axon bundles. The second are the column-like local circuit patterns that stand orthogonal to the lamina-like areas. Such an architecture is reminiscent in its appearance in the mammalian cortex as shown for rodent, vervet monkey and human brains (*12, 16*) Indeed, the thalamopallial input zones of both hyperpallium and DVR are thin, granular neuronal sheets that histologically resemble cortical layer IV and project orthogonally to adjacent pallial areas (*1, 8–10, 17*). Overall, we discovered an organization in which the entire avian sensory pallium is organized in multiple layer-like entities with orthogonally oriented point-to-point bottom-up or top-down projecting circuits. Some cell populations in this system give rise to horizontal projections to neighboring columns or higher-order associative and motor pallial areas. This connectional blueprint was observed across sensory modalities and in both DVR and hyperpallium (*7–10, 14, 18, 19*). Since we found only minor differences between the distantly related owls and pigeons, we propose to label this organization a cortex-like repetitive canonical circuit in the avian forebrain (*20–22*).

The sensory systems of both DVR and hyperpallium are topographically organized as shown for trigeminal BAS (*23*), auditory field L (*24*); somatosensory IHA (*25*), and visual IHA (*26*). The situation is more complicated for entopallium since its thalamic input nucleus consists of several functionally heterogeneous channels (*27, 28*). Since each of them receives retinotopically organized tectal input (*27, 28*) and topography is maintained along the ascending projection (*29*), the entopallium presumably consists of several retinotopically organized subsystems. Thus, each primary sensory DVR

and hyperpallium domain is topographically organized. Since the neurons of these primary sensory zones project in parallel bundles to adjacent nido-, hyper, and mesopallial areas, it is likely that topography is maintained throughout the vertically organized reciprocal circuits of these systems. Indeed, this has been shown for field L (*30*).

Such a pattern is reminiscent of cortical columns that run perpendicular to the topographically organized sensory input layers (*21*). The columnar microcircuits of the neocortex show projections of granular layer IV to supragranular and, to a smaller extent, infragranular layers (*20, 22*), while receiving little excitatory backprojections that mostly stem from layer VI (*31, 32*). Layer II/III neurons have widespread horizontal connections to other columns and cortical areas, as well as vertically oriented projections to striatum and layers V/VI (*29*). Cells from these layers project to various subcortical and some distal cortical areas, but also reciprocate with supragranular layers (*20, 22, 31*).

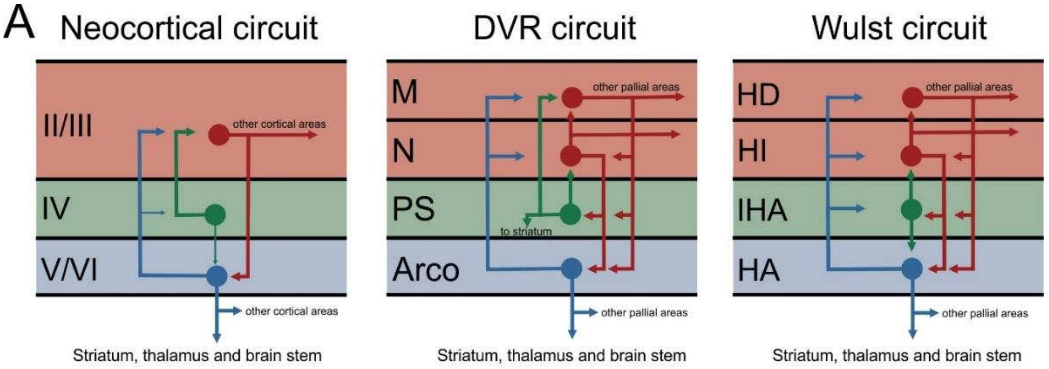

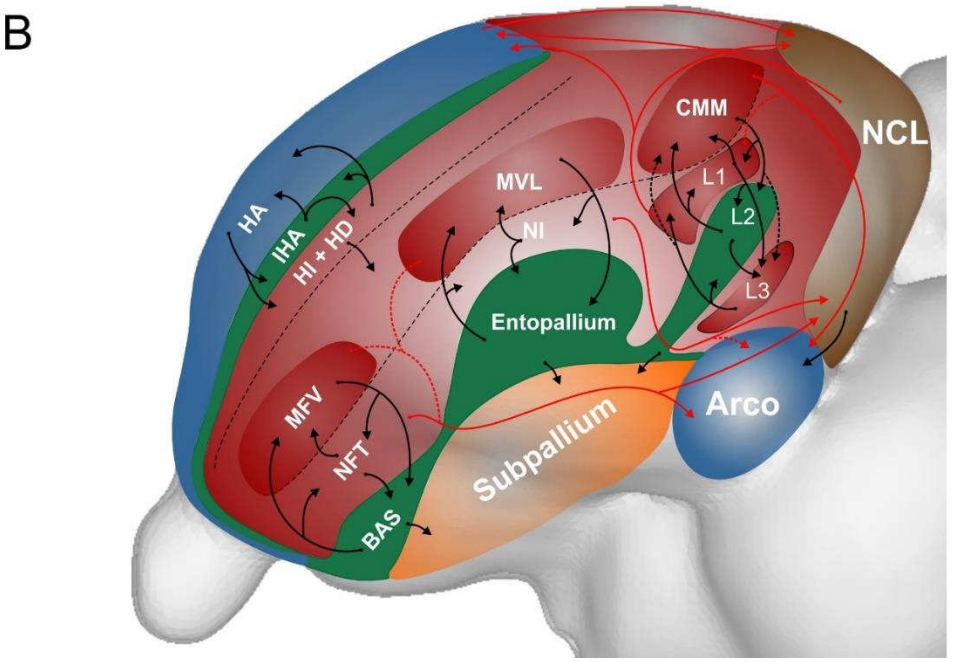

Figure 6) **The canonical circuit and organization of the avian pallium.** A) Simplified canonical circuitries of the mammalian cortex as well as the avian DVR and hyperpallium. Color codes outline putative

correspondences between cortical layers and layer-like entities in birds (primary sensory areas, PS; arcopallium, Arco). B) Summary of the intra-telencephalic sensory connectivity. Black lines represent local, and red lines long-range connections. Dotted lines are connections known from previous studies (*7, 8, 10, 19*).

The summary shown in Fig. 6 demonstrates that organization of the avian pallium exhibits both similarities and differences to neocortex (Fig. 6A). While cortical layer IV cells receive modest excitatory feedback from other layers (*31, 32*), the avian hyperpallial and DVR input zones receive extensive back projections. Additionally, some avian wiring properties like the striatal projections of DVR sensory input neurons and the absence of direct descending projections from the sensory DVR circuit differ from mammals (*20, 22*). On the other hand, there are a large number of parallels between cortex and avian sensory pallium. First, like cortical areas (*21*), and as shown for visual (*8, 9*) and auditory DVR (*10*), avian hyperpallial and DVR sensory systems are organized in columns that link a specific topographical input to a repetitive, vertically oriented processing chains of diverse cell types with archetypical projections. Second, horizontal projections to nearby columns and to distant associative and motor structures arise from selected layer-like areas of hyperpallium and DVR. Third, comparable to cortical canonical microcircuits, hyperpallial and DVR circuits show modest variations between sensory systems and species (*33*). Consequently, computational strategies and dynamics for multiple types of information across sensory systems could be similar in birds and mammals (*34, 35*). Indeed, analyses of single unit activity patterns in the auditory DVR of zebra finches discovered a large number of similar coding principles to neocortex (*30*).

Our results accord in general with genoarchitectonic analysis that distinguish granular, supragranular and infragranular avian pallial territories and indicate that meso- and nidopallium are mirror-like continuous with hyperpallial layers during development (*2, 36*). The presence of genetic markers of different cell types of neocortical layers in birds and reptiles further underline the idea of cell type homologies between major parts of the avian pallium and neocortex (*1, 6, 37, 38*). Thus, it is conceivable that a core common microcircuit already existed in the pallium of the last common stem amniote ancestor and was subsequently modified within mammalian and avian lineages. Since the lateral pallium of lampreys also harbors a three-layered circuit with a ventral sensory input and a dorsal motor output layer, the laminated pallium of extant amniotes may even stem from a far more ancient ancestor (*39*).

We obviously cannot exclude the possibility that both mammals and birds independently developed similar pallial microcircuits by means of convergent evolution. But independent from discussions on the evolutionary origin of the avian pallial canonical microcircuit, our results provide an explanation

for the question of how mammals and birds are able to generate so similar perceptual and cognitive feats (*40*). Our data make it likely that similar microcircuits process information by comparable computational strategies and therefore achieve largely identical cognitive outcomes from seemingly vastly different forebrains.

References and Notes

1. H. J. Karten, Vertebrate brains and evolutionary connectomics. *Philosophical transactions of the Royal Society of London. Series B, Biological sciences*. **370** (2015), doi:10.1098/rstb.2015.0060.
2. E. D. Jarvis, J. Yu, M. V. Rivas, H. Horita, G. Feenders *et al.,* Global view of the functional molecular organization of the avian cerebrum. *The Journal of Comparative Neurology*. **521**, 3614–3665 (2013), doi:10.1002/cne.23404.
3. L. Puelles, J. E. Sandoval, A. Ayad, R. del Corral, A. Alonso *et al.,* The Pallium in Reptiles and Birds in the Light of the Updated Tetrapartite Pallium Model, in *Evolution of Nervous Systems*, J. H. Kaas, Ed. (Elsevier Science, Saint Louis, ed. 2, 2017), pp. 519–555.
4. L. Medina, M. Bupesh, A. Abellán, Contribution of genoarchitecture to understanding forebrain evolution and development, with particular emphasis on the amygdala. *Brain, Behavior and Evolution*. **78**, 216–236 (2011), doi:10.1159/000330056.
5. S. D. Briscoe, C. W. Ragsdale, Homology, neocortex, and the evolution of developmental mechanisms. *Science (New York, N.Y.)*. **362**, 190–193 (2018), doi:10.1126/science.aau3711.
6. S. D. Briscoe, C. B. Albertin, J. J. Rowell, C. W. Ragsdale, Neocortical Association Cell Types in the Forebrain of Birds and Alligators. *Current biology : CB*. **28**, 686-696.e6 (2018), doi:10.1016/j.cub.2018.01.036.
7. M. Shanahan, V. P. Bingman, T. Shimizu, M. Wild, O. Güntürkün, Large-scale network organization in the avian forebrain. *Frontiers in computational neuroscience*. **7**, 89 (2013), doi:10.3389/fncom.2013.00089.
8. M. Fernández, C. Morales, E. Durán, S. Fernández-Colleman, E. Sentis *et al.,* Parallel organization of the avian sensorimotor arcopallium: Tectofugal visual pathway in the pigeon (Columba livia). *The Journal of Comparative Neurology*. **528**, 597–623 (2020), doi:10.1002/cne.24775.
9. P. Ahumada-Galleguillos, M. Fernandez, G. J. Marin, J. C. Letelier, J. Mpodozis, Anatomical organization of the visual dorsal ventricular ridge in the chick (Gallus gallus). *The Journal of Comparative Neurology*. **523**, 2618–2636 (2015), doi:10.1002/cne.23808.
10. Y. Wang, A. Brzozowska-Prechtl, H. J. Karten, Laminar and columnar auditory cortex in avian brain. *Proc Natl Acad Sci USA*. **107**, 12676–12681 (2010), doi:10.1073/pnas.1006645107.
11. C. Herold, P. Schlömer, I. Mafoppa-Fomat, J. Mehlhorn, K. Amunts *et al.,* The hippocampus of birds in a view of evolutionary connectomics. *Cortex*. **118**, 165–187 (2019), doi:10.1016/j.cortex.2018.09.025.
12. M. Axer, S. Strohmer, D. Gräßel, O. Bücker, M. Dohmen *et al.,* Estimating Fiber Orientation Distribution Functions in 3D-Polarized Light Imaging. *Front. Neuroanat.* **10**, 40 (2016), doi:10.3389/fnana.2016.00040.
13. H. J. Karten, W. Hodos, *A stereotaxic atlas of the brain of the pigeon, Columba livia* (Johns Hopkins Press, Baltimore, 1967).
14. J. M. Wild, J. J. Arends, H. P. Zeigler, Telencephalic connections of the trigeminal system in the pigeon (Columba livia). *The Journal of Comparative Neurology*. **234**, 441–464 (1985), doi:10.1002/cne.902340404.
15. G. Zhang, C. Li, Q. Li, B. Li, D. M. Larkin *et al.,* Comparative genomics reveals insights into avian genome evolution and adaptation. *Science (New York, N.Y.)*. **346**, 1311–1320 (2014), doi:10.1126/science.1251385.

16. K. Zilles, D. Gräßel, N. Palomero-Gallagher, P. Schlömer, M. Cremer *et al.,* High-resolution fiber tract imaging using polarized light microscopy in the human, monkey, rat and mouse brain, in *Axons and Brain Architecutre* (Elsevier Acadamic Press, San Diego, 2016), pp. 369–389.
17. H. J. Karten, W. Hodos, W. J. Nauta, A. M. Revzin, Neural connections of the "visual wulst" of the avian telencephalon. Experimental studies in the pigeon (Columba livia) and owl (Speotyto cunicularia). *The Journal of Comparative Neurology*. **150**, 253–278 (1973), doi:10.1002/cne.901500303.
18. T. Shimizu, K. Cox, H. J. Karten, Intratelencephalic projections of the visual wulst in pigeons (Columba livia). *The Journal of Comparative Neurology*. **359**, 551–572 (1995), doi:10.1002/cne.903590404.
19. S. Kröner, O. Güntürkün, Afferent and efferent connections of the caudolateral neostriatum in the pigeon (Columba livia). *The Journal of Comparative Neurology*. **407**, 228–260 (1999), doi:10.1002/(sici)1096-9861(19990503)407:2<228::aid-cne6>3.0.co;2-2.
20. R. J. Douglas, K. A. C. Martin, Neuronal circuits of the neocortex. *Annual Review of Neuroscience*. **27**, 419–451 (2004), doi:10.1146/annurev.neuro.27.070203.144152.
21. V. B. Mountcastle, The columnar organization of the neocortex. *Brain : a journal of neurology*. **120 (Pt 4)**, 701–722 (1997), doi:10.1093/brain/120.4.701.
22. K. D. Harris, G. M. G. Shepherd, The neocortical circuit. *Nature neuroscience*. **18**, 170–181 (2015), doi:10.1038/nn.3917.
23. J. M. Wild, M. F. Kubke, C. E. Carr, Tonotopic and somatotopic representation in the nucleus basalis of the barn owl, Tyto alba. *Brain, Behavior and Evolution*. **57**, 39–62 (2001), doi:10.1159/000047225.
24. D. Bonke, H. Scheich, G. Langner, Responsiveness of units in the auditory neostriatum of the guinea fowl (Numida meleagris) to species-specific calls and synthetic stimuli. *Journal of Comparative Physiology*. **132**, 243–255 (1979), doi:10.1007/BF00614496.
25. P. R. Manger, G. N. Elston, J. D. Pettigrew, Multiple maps and activity-dependent representational plasticity in the anterior Wulst of the adult barn owl (Tyto alba). *The European Journal of Neuroscience*. **16**, 743–750 (2002), doi:10.1046/j.1460-9568.2002.02119.x.
26. J. D. Pettigrew, Binocular visual processing in the owl's telencephalon. *Proceedings of the Royal Society of London. Series B, Biological sciences*. **204**, 435–454 (1979), doi:10.1098/rspb.1979.0038.
27. G. Marin, J. C. Letelier, P. Henny, E. Sentis, G. Farfan *et al.,* Spatial organization of the pigeon tectorotundal pathway. *The Journal of Comparative Neurology*. **458**, 361–380 (2003), doi:10.1002/cne.10591.
28. B. Hellmann, O. Güntürkün, Structural organization of parallel information processing within the tectofugal visual system of the pigeon. *The Journal of Comparative Neurology*. **429**, 94–112 (2001), doi:10.1002/1096-9861(20000101)429:1<94::aid-cne8>3.0.co;2-5.
29. F. Fredes, S. Tapia, J. C. Letelier, G. Marín, J. Mpodozis, Topographic arrangement of the rotundo-entopallial projection in the pigeon (Columba livia). *The Journal of Comparative Neurology*. **518**, 4342–4361 (2010), doi:10.1002/cne.22460.
30. A. Calabrese, S. M. N. Woolley, Coding principles of the canonical cortical microcircuit in the avian brain. *Proc Natl Acad Sci USA*. **112**, 3517–3522 (2015), doi:10.1073/pnas.1408545112.
31. D. Feldmeyer, Excitatory neuronal connectivity in the barrel cortex. *Front. Neuroanat.* **6**, 24 (2012), doi:10.3389/fnana.2012.00024.
32. R. J. Douglas, K. A. C. Martin, Recurrent neuronal circuits in the neocortex. *Current biology*. **17**, R496-500 (2007), doi:10.1016/j.cub.2007.04.024.

33. A. Goulas, P. Majka, M. G. P. Rosa, C. C. Hilgetag, A blueprint of mammalian cortical connectomes. *PLoS biology*. **17**, e2005346 (2019), doi:10.1371/journal.pbio.2005346.
34. G. Hahn, A. Ponce-Alvarez, G. Deco, A. Aertsen, A. Kumar, Portraits of communication in neuronal networks. *Nature reviews. Neuroscience*. **20**, 117–127 (2019), doi:10.1038/s41583-018-0094-0.
35. K. D. Harris, T. D. Mrsic-Flogel, Cortical connectivity and sensory coding. *Nature*. **503**, 51–58 (2013), doi:10.1038/nature12654.
36. C.-C. Chen, C. M. Winkler, A. R. Pfenning, E. D. Jarvis, Molecular profiling of the developing avian telencephalon. *The Journal of Comparative Neurology*. **521**, 3666–3701 (2013), doi:10.1002/cne.23406.
37. I. K. Suzuki, T. Hirata, A common developmental plan for neocortical gene-expressing neurons in the pallium of the domestic chicken Gallus gallus domesticus and the Chinese softshell turtle Pelodiscus sinensis. *Front. Neuroanat.* **8**, 20 (2014), doi:10.3389/fnana.2014.00020.
38. J. Dugas-Ford, J. J. Rowell, C. W. Ragsdale, Cell-type homologies and the origins of the neocortex. *Proc Natl Acad Sci USA*. **109**, 16974–16979 (2012), doi:10.1073/pnas.1204773109.
39. S. M. Suryanarayana, J. Pérez-Fernández, B. Robertson, S. Grillner, The evolutionary origin of visual and somatosensory representation in the vertebrate pallium. *Nat Ecol Evol*. **392**, 917 (2020), doi:10.1038/s41559-020-1137-2.
40. O. Güntürkün, T. Bugnyar, Cognition without Cortex. *Trends in Cognitive Sciences*. **20**, 291–303 (2016), doi:10.1016/j.tics.2016.02.001.
41. M. Axer, D. Grässel, M. Kleiner, J. Dammers, T. Dickscheid *et al.,* High-resolution fiber tract reconstruction in the human brain by means of three-dimensional polarized light imaging. *Front. Neuroinform.* **5**, 34 (2011), doi:10.3389/fninf.2011.00034.
42. M. Axer, K. Amunts, D. Grässel, C. Palm, J. Dammers *et al.,* A novel approach to the human connectome: ultra-high resolution mapping of fiber tracts in the brain. *NeuroImage*. **54**, 1091–1101 (2011), doi:10.1016/j.neuroimage.2010.08.075.
43. R. C. Jones, A New Calculus for the Treatment of Optical SystemsI Description and Discussion of the Calculus. *J. Opt. Soc. Am.* **31**, 488 (1941), doi:10.1364/JOSA.31.000488.
44. M. Menzel, K. Michielsen, H. de Raedt, J. Reckfort, K. Amunts *et al.,* A Jones matrix formalism for simulating three-dimensional polarized light imaging of brain tissue. *Journal of the Royal Society, Interface*. **12**, 20150734 (2015), doi:10.1098/rsif.2015.0734.
45. J. Reckfort, New Approaches to the Interpretation of 3D-Polarized Light Imaging Signals for an Advanced Extraction of Fiber Orientation, thesis, Bergische Universität Wuppertal, Germany.

Acknowledgements

We thank Elisa Wiebeck for support with histology, Christian Schramm for 3D-PLI slice preparations, Philipp Schlömer for support with 3D-PLI images and Sabine Kesch for animal care. We gratefully acknowledge the computing time granted through JARA-HPC on the supercomputer JURECA at Forschungszentrum Jülich.

Funding

Funded by the Deutsche Forschungsgemeinschaft (DFG, German Research Foundation) trough project A01 316803389 (SFB 1280) and project number Neu04 395940726 (SFB 1372) to O.G. The 3D-PLI related part of the presented study was supported by the European Union's Horizon 2020 Research and Innovation Program under Grant Agreement No. 785907 (Human Brain Project, SGA2) to K.A.

Author contributions

M.S., C.H., and O.G. conceived the experiments, M.S. performed the in vivo anatomical tracing, M.S., N.R. and H.W. performed in vitro anatomical tracing, M.S. and C.H. analyzed the data, C.H. performed the 3D-PLI experiments, C.H. and M.A. processed the 3D-PLI data, M.S., C.H., K.A., H.W. and O.G. wrote the manuscript. All authors have read and approved the final manuscript.

Declaration of interest

The authors declare no competing interests.

Data and material availability

All data is available in the main text or the supplementary materials.

Supplementary Materials:

Materials and Methods

Animals

In total 41 homing pigeons (*Columba livia*) and 9 barn owls *(Tyto furcata*) of both sexes were used. Pigeons were obtained from local breeding stocks, while owls were delivered from the Institute of Zoology (RWTH Aachen). In-vitro studies involved 27 pigeons and 9 barn owls, 10 pigeons were used for combined in-vitro/in vivo, 2 pigeons for in-vivo, and 2 pigeons were used for 3D-PLI. All procedures followed the guidelines of the national institutes for the care and the use of laboratory animals and were approved by the animal ethics committee of the State North Rhine-Westphalia (LANUV).

In-vivo tracer application and surgical procedure

Birds were anaesthetized with either a mixture of ketamine and xylazine or with isoflurane combined with the same ketamine/xylazine mixture. The cranial bone was opened and a glass micropipette filled with the Choleratoxin subunit B (CTB, Sigma) was lowered according to stereotactic coordinates (13). 200-400nl tracer was applied using a mechanic pressure device (WPI). After 2 days, birds were used for in-vitro experiments or directly perfused.

In-vitro experiments

For in-vitro tracing, birds were first anesthetized and perfused with ice-cooled sucrose-substituted Krebs solution. Brains were quickly dissected, submerged in this solution for 2min, and cut into 800µm frontal slices with a vibratome. Slices were collected in an artificial cerebro-spinal fluid (ACSF) and continuously oxygenized with carbogen at room temperature. For injections, biocytin crystals (Santa Cruz) were deposited on the desired area using a glass micropipette. Slices were continuously carbogenized in ACSF (4-6h), immersed in 4% paraformaldehyde in 0.12M PB for 12 hours, cryoprotected in 30% sucrose PBS, re-sectioned on a freezing microtome (35µm), and processed according to DAB or fluorescence protocols (see below).

Histology and Immunohistochemistry

Perfusion and brain slicing

Pigeons subjected to in-vivo injections were deeply anesthetized with equithesin and perfused transcardially with 0.9% NaCl followed by cooled (4°C) 4% paraformaldehyde in 0.12M PB. Brains were post-fixated in 4% paraformaldehyde with 30% sucrose (4°C), and cryoprotected in sucrose solution (30% in PBS), to the be cut in frontal plane into 30-40µm thick slices using a freezing microtome.

DAB staining

Standard DAB staining procedure intensified with nickel and cobalt was used to visualize biocytin (*28*). To combine biocytin with CTB staining, the two tracers were stained with and without nickel and cobalt intensification, respectively to obtain black-brown biocytin/CTB double staining. When nickel and cobalt intensification were used, slices were washed in 0.1M sodium acetate buffer (pH 6.0) before transferring into DAB solution.

Fluorescence staining

Slices were incubated in 10% normal horse serum (30 min, Vector ABC kit; in PBST), incubated in polyclonal goat anti-CTB antibody (Sigma-Aldrich; 1:50.00 in PBST) for 72h, rinsed and incubated in a mixture of the secondary antibody Alexa-488 donkey anti-goat (Invitrogen; 1:1.000 in PBST) and Alexa-594 streptavidin (Invitrogen; 1:1.000 in PBST) for 60min. Streptavidin was used to visualize biocytin, conjugated to a fluorophore.

Microscopy and analysis

Slices were analyzed with a ZEISS Imager M1 AXIO microscope equipped with an AxioCam MRm ZEISS 60N-C 2/3'' 0.63x camera and ZEISS filter sets 45 (excitation: BP560/40, beam splitter: FT585, emission: BP630/75) and 38 (excitation: BP470/40, beam splitter: FT495, emission: BP525/50). Color, contrast and brightness adjustments were accomplished via the AxioVision software. Confocal analysis was performed with the LSM 510 (Zeiss) using a Zeiss 40x (Plan-Neofluar, NA 1.3) oil immersion lenses.

3D Polarized Light Imaging (3D-PLI)

3D-PLI is an optical microscopy technique that allows to resolve three-dimensional nerve fibers and fiber tracts in unstained brain sections at microscopic resolution (*41, 42*). The spatial orientations of the nerve fibers are derived from birefringence measurements in histological sections with a polarimetric setup. Birefringence is an optical effect that is mainly caused by myelinated nerve fibers with their highly ordered arrangement and the regular molecular structure of the myelin sheaths surrounding axons. This leads to a so-called negative birefringence with respect to the fiber direction.

<u>Tissue pre-processing</u>

Pigeons (n=2) were euthanized with Pentobarbital (70mg/kg), decapitated, brains were immediately fixed in 4% buffered formalin pH7 and stored at 4°C. They were then transferred into 10% Glycerin, 2% DMSO and 4% formalin pH7 for five days, transferred into a solution of 20% Glycerin, 2% DMSO and 4% formalin pH7 for two weeks, stored at -80°C, and subsequently serially cut with a cryostat in frontal or sagittal planes (thickness 60 μm).

Polarimetric setup, scanning and signal analysis

We used the polarizing microscope TPFM1 (Taorad GmbH, Germany). The device is based on a standard bright field microscope with Köhler illumination (wavelength spectrum 550±5 nm) using one linearly polarizing and one circularly polarizing filter, and a movable specimen stage (Märzhäuser Wetzlar, Germany) that is introduced into the light beam path. The field of view of the built-in monochrome CCD camera (QImaging Retiga 4000R) is 2.7 x 2.7 mm^2 and provides a pixel resolution of 1.3 µm.

Using the movable specimen stage, large-area scans of whole brain sections were carried out tile-wise, with tile overlaps of 1.0 mm or 0.75 mm for frontal and sagittal brain sections, respectively. Each tile was scanned by rotating the linear polarizing filter in equidistant angles (± = 10° for frontal brain sections and ± = 20° for sagittal brain sections) within the range of ρ = 0° and 170°. By this means stacks of 18 or 9 images, respectively, were acquired for each section tile. The measured intensity profile for an individual pixel across the stack of images describes a sinusoidal curve that depends on the orientation of fibers within this pixel (Fig. S1). The physical description of the light intensity profile was derived from the Jones calculus for linear optics (*43, 44*). Three modalities were determined from the sinusoidal curve in dependence on the rotation angle (ρ):

$$I(\rho) = \frac{Transmittance}{2} \cdot [1 + \sin(2\rho - 2 \cdot Direction) \cdot Retardation]$$

$$Retardation = \sin\left(2\pi \cdot \frac{SectionThickness}{LightWaveLength} \cdot Birefringence \cdot \cos^2(Inclination)\right)$$

Transmittance (arbitrary units) is the mean light transmission intensity through tissue (Fig. S1) and reflects its light extinction caused by scattering and absorption processes. *Retardation* (0-1) is the vertical projection of the cumulative tissue birefringence normalized by the transmittance at a given light wavelength (Fig. S1). *Direction* (0°-180°) is the predominant in-(sectioning-)plane nerve fiber orientation (Fig. S1). The out-of-(sectioning-)plane elevation angle of the nerve fiber is called *Inclination* (Fig. S1) and can be estimated from retardation and transmittance by means of four parameters determined on the basis of their gray value distributions over the whole section:

1) *retmaxwm*: maximum white matter retardation 2) *retmaxgm*: maximum gray matter retardation 3) *tmaxgm*: maximum gray matter transmittance 4) *tmeanwm*: mean transmittance of white matter(*45*). *retmaxgm* accounts for gray matter retardation influence. These parameters determine the relation between retardation and inclination by means of the transmittance:

$$\frac{\sin^{-1}(Retardation)}{\cos^2(Inclination)}$$

$$= \frac{log\left(\frac{tmaxgm}{tmeanwm}\right)}{log\left(\frac{tmaxgm}{Transmittance}\right) \cdot \sin^{-1}\left(retmaxwm + (retmaxgm - retmaxwm) \cdot \frac{Transmittance - tmeanwm}{tmaxgm - tmeanwm}\right)}$$

Fiber orientation maps

Direction, inclination (and tissue/background mask) provide a full set of polar coordinates for the calculation of a 3D-vector array of fiber orientations. The vector data of a single section provided by 3D-PLI are represented by color images called fiber orientation maps (FOMs). A point on the colored surface of a (hemi)sphere represents the color of a corresponding 3D fiber orientation (Fig. S1). Yet a quarter sphere is sufficient, because flat 3D-PLI without tilting the light beam does neither differentiate forward and backward orientation, nor the sign of the fiber inclination (downward or upward). Hue corresponds to the direction of the in-plane projection of the fiber orientation. Fiber inclination is coded by saturation and brightness (Fig. S1). In case of the RGB-color-code hemisphere fiber orientations are reflected by colors only. The principal directions (left-right, up-down, front-rear) correspond to fundamental colors (red, green, blue). In the HSV-color-code hemisphere, fiber orientations are reflected by hue, saturation and brightness. In the HSV-black version the brightness decreases with increasing inclination, coloring the poles at 90 degrees black.

Sometimes, the reference for a single vector representation is not a single fiber but all birefringent tissue compartments inside a volume element (voxel) contribute to the signal of an individual image pixel. There are two reasons for signal loss: fiber crossings and steep fibers with inclinations nearby 90°. Therefore, in areas of massive fiber intermingling at scales below the section thickness of 60µm, the direct representation of the fiber orientation by color and saturation is replaced by an extinction texture. Hence, fibers stay visible in the FOM, however, orientation values are getting lost.

Supplementary Figures

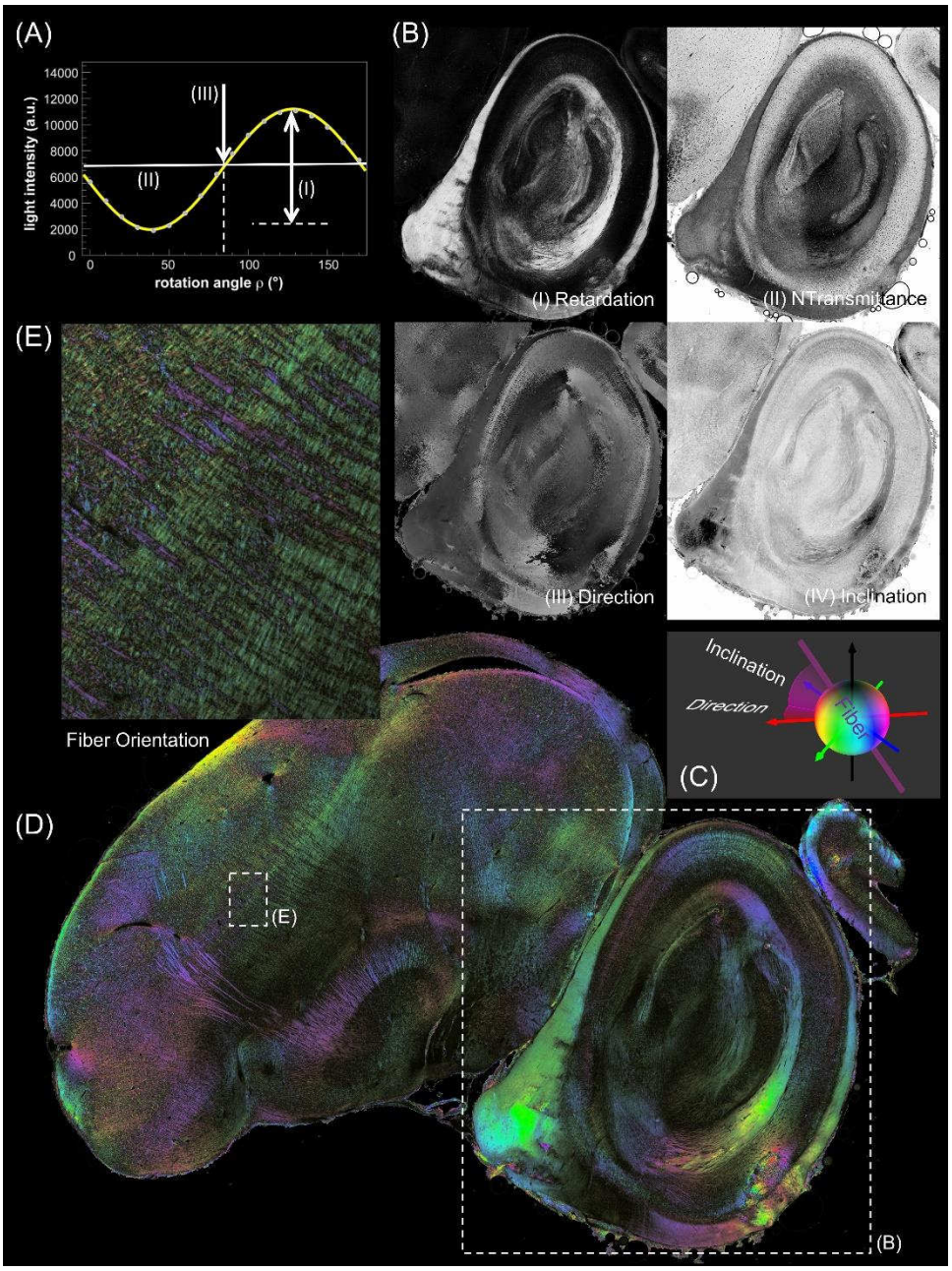

Figure S1) **Data processing pipeline of 3D-PLI at a glance.** (A) The polarimetric measurements yield for each section voxel (here, defined by 1,3 μm × 1,3 μm × 60 μm) one sinusoidal light intensity profile characterizing the transmitted light intensity as a function of the polarizing filter rotation (ρ). HPC-based curve fitting allows to extract three essential 3D-PLI modality maps: Retardation (B.I), NTransmittance (B.II), and Direction (B.III). The Inclination (B.IV) angle is derived from a combined analysis of NTransmittance and Retardation values as detailed in the Materials and Methods section. (C) Direction and Inclination values build a full set of polar coordinates that describe the 3D orientation of the birefringent (fiber) structure by means of an orientation vector. Each derived orientation has its corresponding point on a colored surface of a unit (hemi-)sphere, thus assigning 3D orientation to color

(saturation and brightness encode the fiber inclination). (D) The color-coded vector data of an entire brain section (here, from a pigeon brain cut along the sagittal plane) is called Fiber Orientation map (FOM). The FOM provides unique contrasts between micro-scale fiber architectures in 3D space. (E) The magnified region of interest clearly reveals a field of crossing fibers and fiber tracts.

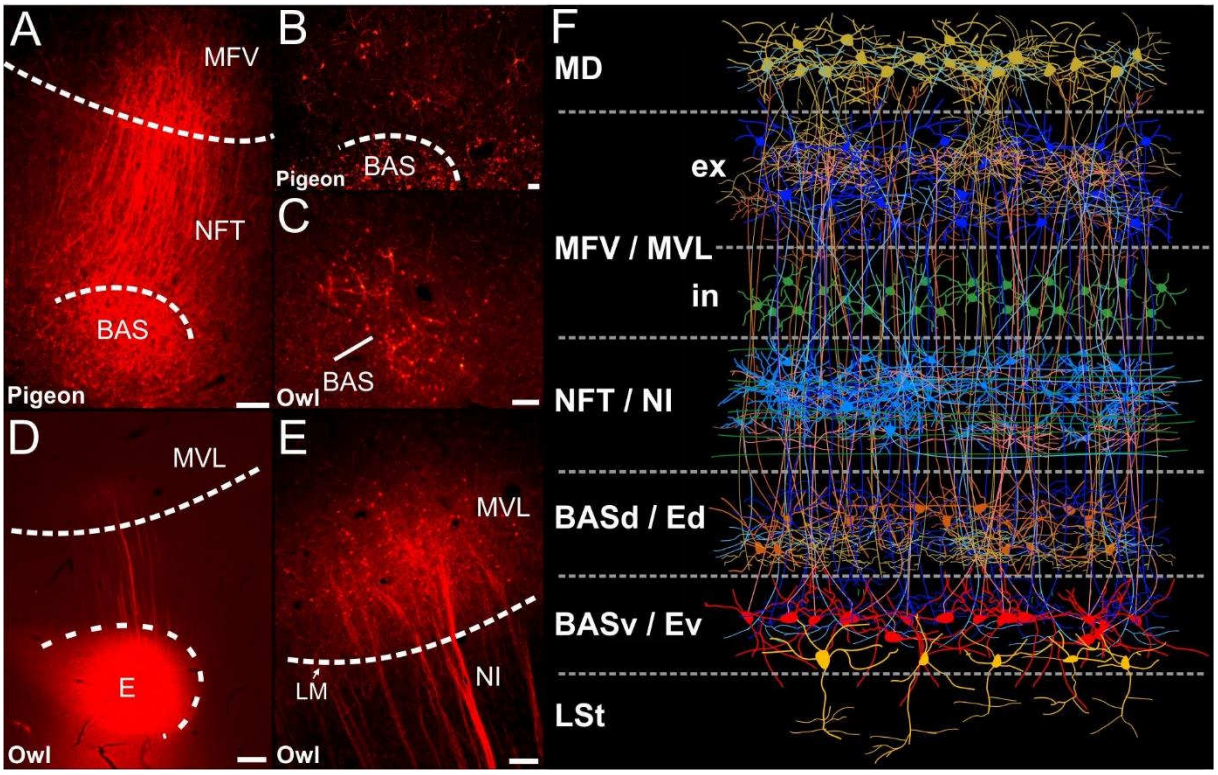

Figure S2: **Local connections within DVR**. The species is indicated on each figure. (A) Vertically oriented fibers emerging from BAS projecting to overlying mesopallium. B) Injections into BAS also labelled neurons in NFT. (C) Retrogradely labelled neurons in BAS after MFV injection. (D) Injection into E in the barn owl with columnar fibers extending into MVL. (E) Fibers and retrogradely labelled neurons in MVL after E injection in the barn owl. (F) Highly schematized depiction of local connections in the trigeminal and visual DVR. Scale bar = 100 µm in A, D; 50 µm in B; Scale bar =100µm in E.